Time-Frequency Representation Of Model Based High Frequency Broad Band Scattering From A Rough Interface

Garner C. Bishop and Judy Smith

Naval Undersea Warfare Center Division Newport
Newport, RI 02841

Abstract

A formalism for scattering a broad band high frequency pulse from a randomly rough surface of a penetrable oceanic sediment is developed and used to investigate the ability of local cosine transform (LCT) time-frequency (TF) representations to distinguish between randomly rough surfaces with different statistics.

1. Introduction

It is of interest to classify surface texture or roughness remotely using broad band acoustic scattering. In this paper, the interest is in classification of roughness on the surface of penetrable oceanic sediments. Previously[1,2], a T-matrix formalism was used to calculate broad band LFM scattering from an elastic sediment with periodic surface roughness. An adaptive windowed local cosine transform (LCT) was used to construct time-frequency (TF) representations of the time series and it was shown that this type of TF representation could distinguish between two different types of periodic roughness. In this paper, high frequency broad band scattering from penetrable sediments with random surface roughness is calculated and the ability of local cosine based TF representations of the scattered field time series to distinguish between rough surfaces with different statistics is explored.

It is assumed that a stationary source array is located in a homogeneous, isotropic, and non-viscous fluid half space bounded below by a semi-infinite penetrable sediment half space with a randomly rough surface. The surface roughness profile $\xi(x',y')$ is assumed to be a realization of a zero mean Gaussian random process with an RMS height h and correlation lengths l_x and l_y along the x- and y-axes. The fluid half space is denoted medium (1) and the sediment half space is denoted medium (2). In the fluid half space, the compressional Lame parameter is $\lambda^{(1)}$, the mass density is $\rho^{(1)}$, the p-wave speed is $c^{(1)\,2}=\lambda^{(1)}/\rho^{(1)}$, and the p-wave vector is $\hat{k}^{(1)}$ with $k^{(1)\,2}=\omega^2/c^{(1)\,2}$. Although scattering from sound hard, viscous fluid, viscoelastic solid, and fluid saturated poroelastic solid sediments was modeled, in this paper, numerical results are shown for a viscoelastic solid only. In the viscoelastic solid sediment, the Lame parameters are $\lambda^{(2)}$ and $\mu^{(2)}$, the mass density is $\rho^{(2)}$, the p and s wave speeds are, respectively, $c_p^{(2)\,2}=(\lambda^{(2)}+2\mu^{(2)})/\rho^{(2)}$ and $c_s^{(2)\,2}$ and $c_s^{(2)\,2}=\mu^{(2)}/\rho^{(2)}$, and the p and s wave vectors are, respectively, $\hat{k}_p^{(2)}$ with $k_p^{(2)\,2}=\omega^2/c_p^{(2)\,2}$ and $\hat{k}_s^{(2)}$ with $k_s^{(2)\,2}=\omega^2/c_s^{(2)\,2}$.

It is assumed that the source is a planar array and to orient and locate the array, two coordinate systems are considered: A reference coordinate system is located in the mean plane of the rough interface and is designated $x_i\ y_i\ z_i$ with origin O_i and a second coordinate system is located in the plane of the array and is designated, $x_s\ y_s\ z_s$ with origin O_s. The x_s and y_s axes are in the plane of the array and are parallel, respectively, to the width and length of the array and the z_s axis is normal to the $x_s\ y_s$ plane and in the direction of the main lobe of the beam. Initially both coordinate systems are coincident and colinear. First, the source is displaced from the origin O_i and then it is oriented so that the z_s-axis is along a radius vector $\hat{r}_s$ from O_s to O_i. The rotation of the z_s-axis is accomplished by performing a counterclockwise rotation by an angle ϕ_s about the z_s-axis followed by a second counterclockwise rotation by an angle $\pi+\theta_s$ about the y_s-

axis. In this analysis, the source is located on the negative x_s -axis so that $\phi_s = \pi$.

It is assumed that in the far field the source pressure field can be expressed in the following manner:

$$p^{(i)}(\dot{r},\dot{r}_s;t) = \frac{1}{2\pi}\int_{-\infty}^{\infty} d\omega\, T^{(i)}(\omega)\; p^{(i)}(\dot{r},\dot{r}_s;\omega)\; e^{-i\omega t} \tag{1a}$$

with

$$p^{(i)}(\dot{r},\dot{r}_s;\omega) = P_o\, D_s(\dot{r},\omega)\; e^{ik^{(1)}|\dot{r}-\dot{r}_s|}\;/4\pi|\dot{r}-\dot{r}_s| \tag{1b}$$

The quantity $D_s(\dot{r},\omega)$ is the source beam pattern and in this paper, a Gaussian beam is considered . When $D_s(\dot{r},\omega)$ is projected onto the mean plane of the interface it is given by

$$D_s^{(i)}(\dot{r}';\omega) = \exp[-(x'/X)^2]\exp[-(y'/Y)^2]. \tag{2a}$$

with

$$X = r_s\,\chi/\cos\theta_s\,, \tag{2b}$$

$$Y = r_s\,\phi\,, \tag{2c}$$

$$\chi = k_{min}\,\chi_{max}/k \tag{2d}$$

and

$$\phi = k_{min}\,\phi_{max}/k \tag{2e}$$

The angles χ and ϕ are, respectively, the beam widths measured from the z_s -axis in the z_s -x_s and z_s -y_s planes and the angles, χ_{max} and ϕ_{max} are the maximum values of these angles and occur when $k=k_{min}$. The beam pattern $D_s(\dot{r},\omega)$ is obtaind from $D_s^{(i)}(\dot{r}';\omega)$ by setting $\cos\theta_s = 1$.

The quantity $T^{(i)}(\omega)$ is the Fourier transform of the incident pulse $T^{(i)}(t)$ and in this paper, scattering of a linear frequency modulated (LFM) pulse is considered so that

$$T^{(i)}(t) = \begin{cases} e^{-i\omega(t)t} & 0 \le t \le \tau \\ 0 & t > \tau\,; t < 0 \end{cases} \tag{3}$$

with $\omega(t)=2\pi(f_{min} + t\Delta f/\tau)$. The parameter τ is the pulse width, f_{min} is the lowest frequency in the pulse, and Δf is the bandwidth.

The scattered field is synthesized from its spectrum using an inverse Fourier transform so that

$$p^{(s)}(\dot{r},\dot{r}_s;t) = \frac{1}{2\pi}\int_{-\infty}^{\infty} d\omega\, T^{(i)}(\omega)\, p^{(s)}(\dot{r},\dot{r}_s;\omega)\; e^{-i\omega t} \tag{4}$$

The quantity $p^{(s)}(\dot{r},\dot{r}_s;\omega)$ is the Fourier spectrum of the scattered pressure field and is calculated using a Kirchhoff scattering formalism.

2. Kirchhoff Scattering for a Randomly Rough Interface

2.1 Scattering Theory: CW Scattering

Since scattering from a randomly rough surface in the Kirchhoff approximation has been treated by many authors [3-5], the details of the formalism used in this paper are briefly reviewed. The pressure field scattered from the rough interface is given by the Helmholtz-Kirchhoff integral:

$$p^{(s)}(\dot{r},\dot{r}_s;\omega) = \int ds'\,[p^{(+)}(\dot{r}',\omega)\,\hat{n}(\dot{r}')\cdot\nabla' g(\dot{r}',\dot{r};\dot{k}^{(1)}) - g(\dot{r}',\dot{r};\dot{k}^{(1)})\,\hat{n}(\dot{r}')\cdot\nabla' p^{(+)}(\dot{r}',\omega)\,]. \tag{5}$$

The quantity $p^{(+)}(\dot{r}',\omega)$ is the total field evaluated in the limit in which the interface is approached from the fluid half

space and $g(\dot{r}', \dot{r}; \dot{k}^{(1)})$ is the free space scalar Green function. The vectors $\dot{r}$ and $\dot{r}'$ are, respectively, vectors to a feld point and to a point on the surface. The unit vector $\hat{n}(\dot{r}')$ is normal to the interface and is given by

$$\hat{n}(\dot{r}') = [\hat{z} - \partial_{x'}\xi(x',y')\hat{x} - \partial_{y'}\xi(x',y')\hat{y}]\{1+[\partial_{x'}\xi(x',y')]^2+[\partial_{y'}\xi(x',y')]^2\}^{-\frac{1}{2}} \tag{6}$$

and $ds' = dx'dy'\{1+[\partial_{x'}\xi(x',y')]^2+[\partial_{y'}\xi(x',y')]^2\}^{\frac{1}{2}}$ and is an infinitesimal area element on the interface.

The far-field approximation for the Green function and incident field evaluated on the rough surface are constructed in the Fraunhoffer approximation and are given by

$$p^{(i)}(\dot{r}', \dot{r}_s; \omega) = P_o D_s^{(i)}(\dot{r}'; \omega) e^{i(\dot{k}^{(1)} r_s + \dot{k}^{(i)} \cdot \dot{r}')}/4\pi r_s \tag{7a}$$

and

$$g(\dot{r}', \dot{r}; \dot{k}^{(1)}) = e^{i(\dot{k}^{(1)} r - \dot{k}^{(s)} \cdot \dot{r}')}/4\pi r. \tag{7a}$$

The wave vectors $\dot{k}^{(i)}$ and $\dot{k}^{(s)}$ are , respectively, the wave vectors for the incoming and outgoing waves.

Since scattering from a rough interface in the Fraunhoffer approximation is valid only when the source insonifies a relatively small area on the interface, the interface is located in the far field of the source array with $r_s > A_s/\lambda$ for all frequencies of interest (A_s is the planar area of the source array.), $r'/r_s << 1$, and $r'/r << 1$ for all r'. To be able to maintain the validity of the Fraunhoffer approximation and to obtain a computationally tractable numerical solution, the formalism is limited to narrow beam source arrays.

In the Kirchhoff approximation, it is assumed that the surface field and its normal derivative are given by

$$p^{(+)}(\dot{r}', \omega) = [1+R(\hat{r}', \hat{k}^{(i)})]\, p^{(i)}(\dot{r}', \dot{r}_s; \omega) \tag{8a}$$

and

$$\hat{n}(\dot{r}') \cdot \dot{\nabla}' p^{(+)}(\dot{r}', \omega) = iP_o [1-R(\hat{r}', \hat{k}^{(i)})]\, \dot{k}^{(i)} \cdot \hat{n}(\dot{r}')\, D_s^{(i)}(\dot{r}'; \omega)\, e^{i(\dot{k}^{(1)} r_s + \dot{k}^{(i)} \cdot \dot{r}')}/4\pi r_s . \tag{8b}$$

In Eqs. (8a) and (8b), $R(\hat{r}', \hat{k}^{(i)})$ is the plane wave amplitude reflection coefficient for a planar interface. In this paper, scattering from a viscoelastic solid sediment is calculated so that

$$R(\hat{r}', \hat{k}^{(i)}) = (A-B)/(A+B) \tag{9a}$$

with

$$A = \rho_2 k_z^{(1)} [4k_{pz}^{(2)} k_{sz}^{(2)} k_{px}^{(2)2} + (k_{sz}^{(2)2} - k_{px}^{(2)2})^2], \tag{9b}$$

$$B = \rho_1 k_{pz}^{(2)} \kappa_s^{(2)4}, \tag{9c}$$

$$k_{pz}^{(2)} = \sqrt{\kappa_p^{(2)2} - k_{px}^{(2)2}}, \tag{9d}$$

$$k_{sz}^{(2)} = \sqrt{\kappa_s^{(2)2} - k_{sx}^{(2)2}}, \tag{9e}$$

$$k_{px}^{(2)} = k_{sx}^{(2)} = k_x^{(1)}, \tag{9f}$$

$$\kappa_p^{(2)} = k_p^{(2)} + i\omega\alpha_p/8683, \tag{9g}$$

and

$$\kappa_s^{(2)} = k_s^{(2)} + i\omega\alpha_s/8683. \tag{9h}$$

The quantities $k_p^{(2)}$ and $k_s^{(2)}$ are, respectively, the wave numbers for the pressure and shear waves in the sediment and α_p and α_s are the corresponding log decrement attenuations. It is important to note that since the reflection coefficient depends on the local angle of incidence, it depends on the surface derivative as well as the plane wave angle of incidence. Therefore, when Eqs. (6)-(8) are used in the Helmholtz-Kirchhoff integral, the numerical evaluation of the resulting integral is complicated by the fact that the integrand depends on the surface derivatives. To simplify the evaluation of this

integral, it is assumed that for narrow beams and small surface slopes $R(\hat{r}', \hat{k}^{(i)})$ is approximately constant on the insonified portion of interface and may be evaluated by using the mean angle of incidence at the interface. For isotropic surface roughness, the mean slope angle of the interface is $\gamma = \tan^{-1}(\sqrt{2}\, h/l)$, where l is the correlation length [5]. Then the surface derivatives are eliminated by performing an integration by parts and the resulting expression for the scattered pressure field is

$$p^{(s)}(\dot{r}, \dot{r}_s; \omega) = -ik^{(1)} P_o \frac{e^{ik^{(1)} r_s}}{4\pi r_s} \frac{e^{ik^{(1)} r}}{4\pi r} \int dx'dy' \exp\left\{ ik^{(1)} [Ax'+By'+C\xi(x',y')] \right\} D_s^{(i)}(\dot{r}'; \omega) \left[\frac{aA}{C} + \frac{bB}{C} + c\right]. \quad (10a)$$

with

$$a = \left\{ [1+R(\hat{r}', \hat{k}^{(i)})]\, \hat{k}^{(s)} + [1-R(\hat{r}', \hat{k}^{(i)})]\, \hat{k}^{(i)} \right\}_x , \quad (10b)$$

$$b = \left\{ [1+R(\hat{r}', \hat{k}^{(i)})]\, \hat{k}^{(s)} + [1-R(\hat{r}', \hat{k}^{(i)})]\, \hat{k}^{(i)} \right\}_y , \quad (10c)$$

$$c = \left\{ [1+R(\hat{r}', \hat{k}^{(i)})]\, \hat{k}^{(s)} + [1-R(\hat{r}', \hat{k}^{(i)})]\, \hat{k}^{(i)} \right\}_z , \quad (10d)$$

$$A = (\hat{k}^{(i)} - \hat{k}^{(s)})_x , \quad (10e)$$

$$B = (\hat{k}^{(i)} - \hat{k}^{(s)})_y , \quad (10f)$$

and

$$C = (\hat{k}^{(i)} - \hat{k}^{(s)})_z . \quad (10g)$$

In Eq. (10a), terms involving derivatives of the projected beam pattern have been omitted. For a Gaussian beam, these terms can be omitted when $2k^{(1)} AX >> 1$ and $2k^{(1)} AY >> 1$.

2.2 Rough Surface Realizations

A two dimensional generalization of the technique used by Thorsos[5] was used to construct two dimensional realizations of a rough surface with Gaussian statistics. The surface height is given by

$$\xi(x',y') = \frac{1}{L_x L_y} \sum_{m=-N/2}^{N/2-1} \sum_{n=-N/2}^{N/2-1} F(K_{xm}, K_{yn}) \exp[i(K_{xm} x' + K_{yn} y')] \quad (11a)$$

where the spectral amplitude $F(K_{xm}, K_{yn})$ is given by

$$F(K_{xm}, K_{yn}) = 2\pi \sqrt{L_x L_y W(K_{xm}, K_{yn})} \begin{cases} \cos\phi & \begin{matrix} m=0;N/2 \\ n=0;N/2 \end{matrix} \\ [\cos\phi + i\sin\phi] & \begin{matrix} m\neq 0;N/2 \\ n\neq 0;N/2 \end{matrix} \end{cases} \quad (11b)$$

with $\cos\phi = N_1(0,1)$, $\sin\phi = N_2(0,1)$, $K_{xm} = 2\pi m/L_x$, and $K_{yn} = 2\pi n/L_y$. When $m<0$ or $n<0$, $F(K_{x-m}, K_{y-n}) = F^*(K_{xm}, K_{yn})$ so that $\xi(x',y')$ is real. The lengths L_x and L_y are, respectively, the lengths along the x- and y-axes of the insonified area on the mean plane of the interface, c is the correlation coefficient, and $N_1(0,1)$ and $N_2(0,1)$ are independent samples from a zero mean unit variance Gaussian distribution. The quantity $W(K_{xm}, K_{yn})$ is the two dimensional Gaussian roughness spectrum is given by

$$W(K_{xm}, K_{yn}) = \frac{l_x l_y h^2}{4\pi\sqrt{1-c^2}} \exp\{ -[(l_x x')^2 + (l_y y')^2 - 2c l_x l_y x'y']/4\sqrt{1-c^2} \} \quad (12)$$

and is normalized such that $\int_{-\infty}^{\infty} d\dot{K}\, W(\dot{K}) = h^2$.

3. Adaptive Windowed Local Cosine Transform

An adaptive windowed local cosine transform[7] is used to construct TF representations of the scattered field time series. The time series are segmented or windowed in time so that the resolution in the TF plane is limited by the uncertainty principle which is expressed by the fact that the time-bandwidth product is constant i.e., $\Delta t \Delta f \geq 1$. The time-bandwidth product describes a Heisenberg cell and the ensemble of Heisenberg cells provides a tiling of the TF plane. The TF representation of a signal is displayed graphically in a TF plane in which the Heisenberg cells are shaded in proportion to the TF spectral amplitude:

In this paper, the segmentation or windowing process is used adaptively to construct a near optimal segmentation which is equivalent to a near-optimal localization in time and frequency. An optimal segmentation minimizes the number of large amplitude Heisenberg cells and the shaded area in the graphical display of the T-F representation. To obtain an optimal segmentation in time, the time series is segmented following a dyadic tree structure. The optimal distribution of windows is obtained by comparing the TF representation of the time series using two adjacent intervals with that produced by their union. The optimal window is the one that for a fixed number of largest coefficients maximizes energy or minimizes entropy. An optimal segmentation consists of a distribution of windows obtained from different levels of the dyadic tree and its graphical display is characterized by Heisenberg cells with different aspect ratios. A best level representation is obtained by using an optimal uniform segmentation, i.e., a single level within the dyadic tree structure, and its graphical display is characterized by Heisenberg cells with a constant aspect ratio.

The novel feature of the adaptive windowed LCT used in this paper is the bell shaped window $w_j(t)$ introduced by Coifman and Meyer [8]. On the interval $I_j = [a_j, a_{j+1}]$ with length l_j, $w_j(t)$ satisfies the following conditions:

$$0 \leq w_j(t) \leq 1, \tag{13a}$$

$$w_j(t) = 1 \quad t \in [a_j + \varepsilon_j, a_{j+1} - \varepsilon_{j+1}],$$

$$0 \quad t \notin [a_j - \varepsilon_j, a_{j+1} + \varepsilon_{j+1}], \tag{13b}$$

$$w_j(t) = w_{j-1}(2a_{j+1} - t), \tag{13c}$$

and

$$w_j^2(t) + w_{j-1}^2(t) = 1 \quad |t - a_j| \leq \varepsilon_j . \tag{13d}$$

The windows that satisfy the conditions in (13) extend beyond the interval I_j and provide a smooth and symmetrical overlap with adjacent windows.

The LCT basis functions introduced in [4] are given by

$$u_{j,k}(t) = \sqrt{2/l_j}\ \ w_j(t)\ \cos[\pi(k+1/2)(t-a_j)/l_j]. \tag{14}$$

The basis functions $u_{j,k}(t)$ are orthonormal not only within the interval I_j, but throughout the TF plane. It can be shown that if a function $f(t) \in L^2(R)$, then it can be represented in the following manner:

$$f(t) = \sum_{j=1}^{\infty} \sum_{k=0}^{\infty} c_{j,k}\, u_{j,k}(t) \tag{15a}$$

with

$$c_{j,k} = \int_{a_j - \varepsilon_j}^{a_{j+1} + \varepsilon_{j+1}} dt\, f(t) u_{j,k}(t) = \int_{a_j}^{a_{j+1}} dt s_j(t) \sqrt{2/l_j}\ \cos[\pi(k+1/2)(t-a_j)/l_j] \tag{15b}$$

and

$$s_j(t) = f(t) w_j(t) - f(2a_j - t) w(2a_j - t) + f(2a_{j+1} - t) w_j(2a_{j+1} - t) . \tag{15c}$$

The effect of the window $w_j(t)$ is evident in (15) where it is shown that the energy in the overlap region is folded back into the interval I_j and the function $s_j(t)$ is projected out from f(t) and onto the basis functions. Using the representation given in (15a), a signal can be represented by an optimal TF spectrum that can be used to reconstruct the signal. In addition, the Heisenberg cells are disjoint, there is no energy leakage between adjacent cells, and the uncertainty principle is obeyed.

4. Numerical Considerations and Parameters

When Eqs. (11) and (12) are used to generate a surface realization, l_x , l_y , c, and h are input parameters however, the lengths of the insonified surface area, L_x and L_y , need to be determined. These lengths are given by the values of $x'=L_x/2$ and $y'=L_y/2$ for which the Gaussian beam in the x and y-direction decreases by exp(-3), i.e., when $\exp[-(L_x/2X)^2] = \exp[-(L_y/2Y)^2] = \exp(-3)$ so that $L_x = 2\sqrt{3}\ r_s\ \chi/\cos\theta_s$ and $L_y = 2\sqrt{3}\ r_s\ \phi$. It is important to note that when θ_s or r_s change, the surface realization changes as well. However, in this analysis the same surface realization was used for all calculations and the lengths L_x and L_y were fixed at their values for $\theta_s = 30^\circ$ and $r_s = 20$ m. An FFT was used to calculate a surface realization on a 1024x1024 grid with spatial increments $\Delta x = L_x/1024 < \lambda/5$ and $\Delta y = L_y/1024 < \lambda/5$ [5]. To insure that the minimum spatial sampling $\lambda/5$ was obtained, the number of points $N_x = L_x/(\lambda/5)$ was calculated and if $N_x > 1024$, the calculation was not performed. The same spatial sampling was used to evaluate the integral over the interface.

Although a closed form expression for the Fourier transform of an LFM pulse can be obtained, it was found that the FFT evaluation of $T^{(i)}(\omega)$ was numerically more convenient. The number of time samples is $N = 2^n$ where the integer n is determined by dividing the time window by .he sample frequency. The time window is T and the sample frequency is the reciprocal of twice the highest frequency, i.e., the Nyquist frequency, so that $n = \ln[2(f_{min} + \Delta f)T]/\ln 2 + 1$ and for $= 10\tau$ and the parameters considered in this paper n=17.

Time series were calculated by evaluating the inverse Fourier transform of the product of the incident pulse and interface scattered field spectra. Since the calculation required a large number of spectral samples, the spectrum of the interface scattered field was calculated on 16 nodes of a Cray T3D. It is important to note that the spectrum of the incident pulse is confined to the range of positive frequencies ~22-28 kHz for which the Kirchhoff approximation is valid. So that it is not necessary to calculate interface spectral components for frequencies for which the Kirchhoff approximation is not valid.

A set of parameters was chosen for the source, the fluid half space, the rough surface, and the sediment. These parameters are summarized in Tables 1 and 2. In the following, these parameters remain fixed unless noted otherwise. The parameters for the viscoelastic sediment are for a a sandy sediment for which the p-wave speed is greater than that in the fluid.

5. Results and Conclusions

Time series and local cosine based TF representations were calculated for back scattering with $\theta_s = \theta_r = 30^\circ$ from surfaces with h=0.01 m and h=0.1 m with $l_x = l_y = 0.1$ m, 0.5 m, and 1.0 m. Figure 1 shows TF representations for scattering from surfaces with h=0.01 m and (a1) l=0.01m, (a2) l=0.5 m, and (a3) l=1.0. Figures (b1)-(b3) show similar results for surfaces between randomly rough surfaces with different statistics, i.e., rms surface heights and correlation lengths. In general, differences in the TF representations of the scatter from statistically different surfaces are not dramatic, however, differences are most apparent in the high frequency portion of the TF plane. This suggests that classification of randomly rough surfaces may be facilitated by broad band pulses whose spectrum includes frequencies higher than those considered here.

It may be concluded that LCT based TF representations of broad band time series scattered from randomly rough surfaces affect a data compression of the time series and that in the TF plane, scattering from randomly rough surfaces with different statistics can be distinguished. Although no attempt has been made to develop an algorithm to classify surface roughness, the results shown here indicate that it may be useful to consider local cosine based TF representations as a basis for an algorithm to classify surface roughness.

References

[1] G. C. Bishop and Q. Huynh,"Time-Frequency Analysis of Model Based Pulse Scattering from a Fluid-Elastic Interface with Periodic Roughness," in Proceedings of Oceans '94, 13-16 Sept. 1994, Brest, France, Vol. II, 521-526.

[2] G. C. Bishop and J. Smith, "A T-matrix for scattering from a doubly infinite doubly periodic fluid-solid interface with periodic surface roughness," J. Acoust. Soc. Am. **94**, 1560-1583 (1993).

[3] P. Beckmann and A. Spizzichino, *The Scattering of Electromagnetic Waves from Rough Surfaces*, (The Macmillan Company, New, York, 1963), Ch. 3.

[4] J. Ogilvy, *Theory of Wave Scattering from Random Rough Surfaces*, (Adam Hilger, New York, NY, 1991), Ch. 4.

[5] E. Thorsos, "The validity of the Kirchhoff approximation for rough surface scattering using a Gaussian roughness spectrum," J. Acoust. Soc. Am., **83**, 78-92, (1987).

[6] G. C. Bishop and J. Smith, "High frequency scattering from a target in proximity to a randomly rough interface," unpublished.

[7] R. R. Coifman, Y. Meyer, and M. V. Wickerhauser, "Wavelet analysis and signal processing," in *Wavelets and their Applications*, M. Ruskal et al., (eds.), (Jones and Bartlett, Boston, Ma, 1992), pp. 153-178.

[8] R. R. Coifman and Y. Meyer, "Remarques sur l'analyse de Fourier a fenetre," C. R. Acad. Sci., Ser. 1, 312, 259-261, (1991).

[9] G. Frisk, *Ocean And Seabed Acoustics*, (PTR Prentice Hall, Englewood Cliffs, NJ, 1994), p. 50.

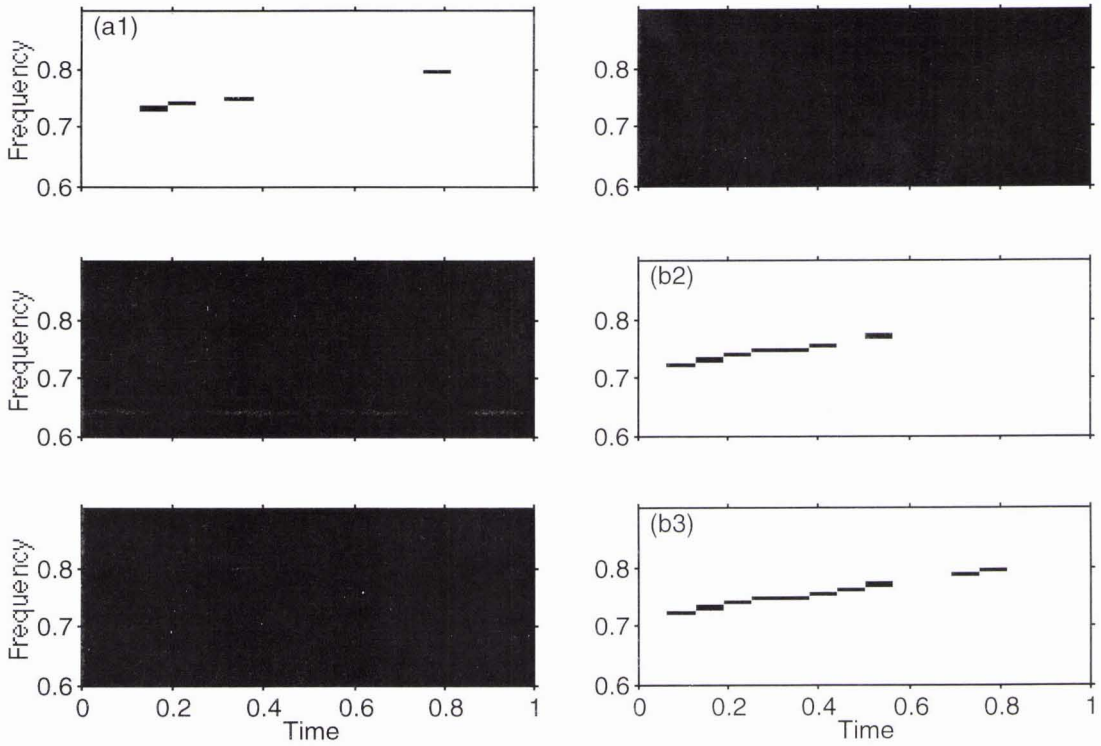

Fig. 1. Local cosine transform time-frequency representations of LFM scattering from randomly rough surfaces with h=0.01 m and (a1) l=0.1 m, (a2) l=0.5 m, and (a3) l=1.0 m and with h=0.1 m and (b1) l=0.1 m, (b2) l=0.5 m, and (b3) l=1.0 m.

Table 1. Source and receive parameters.

	symbol	parameter	value
source			
	P_o	incident amplitude	4π
	r_s	distance	20 m
	θ_s	polar angle	30^o
	ϕ_s	azimuthal angle	180^o
	χ_{max} , ϕ_{max}	beam widths	4^o
	D_s	beam pattern	Gaussian
	t	pulse width	0.2 s
	f_{min}	min frequency	23.75 kHz
	Δf	band width	2.5 kHz
receive			
	r_r	distance	20 m
	θ_r	polar angle	30^o
	θ_r	azimuthal angle	180^o

Table 2. Fluid, sediment, and roughness parameters.

	symbol	parameter	value
sfluid			
	$c_p^{(1)}$	sound speed	1500 m/s
	$\rho_f^{(1)}$	fluid density	1000 kg/m^3
sediment[9]			
	$c_p^{(2)}$	p-wave speed	1478.0 m/s
	$\alpha_p^{(2)}$	p-wave attenuation	0.07 dB/m/kHz
	$c_s^{(2)}$	s-wave speed	121.83 m/s
	$\alpha_s^{(2)}$	s-wave attenuation	4.474 dB/m/kHz
	$\rho^{(2)}$	density	1800.0 kg/m^3
roughness			
	h	mean height	0.01 m
	$l_x = l_y = l$	correlation length	0.5 m
	c	correlation coefficient	0